Numerical Study of the Impact of Vibration Localization on the Motional Resistance of Weakly Coupled MEMS Resonators

Andreja Erbes, *Student Member, IEEE,* Pradyumna Thiruvenkatanathan, *Member, IEEE,* Jim Woodhouse and Ashwin A. Seshia, *Senior Member, IEEE*

***Abstract*—This paper presents a numerical study of the impact of process-induced variations on the achievable motional resistance R_x of one-dimensional, two-dimensional, cyclic and cross-coupled architectures of weakly coupled, electrostatically transduced MEMS resonators operating in the 250 kHz range. We use modal analysis to find the R_x of such coupled arrays and express it as a function of the eigenvectors of the specific mode of vibration. Monte Carlo numerical simulations, which accounted for up to 0.75% variation in critical resonator feature sizes, were initiated for different array sizes and coupling strengths, for the four distinct coupling architectures. Improvements in the mean and standard deviation of the generated R_x distributions are reported when the resonators are implemented in a cross-coupled scheme, as opposed to the traditional one-dimensional chain. The two-dimensional coupling scheme proves to be a practical and scalable alternative to weakly coupled one-dimensional chains to improve the immunity to process variations. It is shown that a 75% reduction in both the mean and standard deviation of the R_x is achieved as compared to the traditional one-dimensional chain for a normalized internal coupling $\kappa > 10^{-2}$.**

***Keywords*—Mechanical coupling, motional resistance, vibration localization, mode localization, MEMS resonators.**

I. Introduction

The demand for high performance and reduced size wireless communication devices has pushed research interests towards the design and development of low power, small footprint and single chip CMOS integrated wireless-transceiver solutions. The potential of Micro Electro Mechanical Systems (MEMS) technology to meet some of these requirements has led to the recent development and adoption of miniaturized, silicon micro-machined mechanical resonators for operation as timing references [1]. Such micro-resonators, unlike their traditional quartz crystal counterparts, are manufactured using silicon micro-fabrication techniques and offer considerably smaller form factor as well as shorter lead time. Electrostatically transduced silicon MEMS resonators have also been shown to provide a number of advantages including - high mechanical quality factors (Q), low static power dissipation and CMOS manufacturing compatibility, making them attractive alternatives to quartz based timing references. However, such silicon micro-resonators are still limited by their high motional resistance (R_x) that consequently hinders direct deployment in RF front-end applications.

One-dimensional (1D-κ) mechanical coupling of micro-resonators (see discrete element model in Fig. 1a) has been suggested as a potential route to reduce the R_x of such devices [2][3]. At high frequencies, coupling beams designed to be integer number of half-wavelengths can be used to implement very strong coupling between resonators. However, for VLF-MF flexural mode resonators, it can become impractical to implement strong extensional or flexural mode coupling beams due to size constraints (e.g. such $\frac{\lambda}{2}$ couplers would require hundreds of microns long beams at the operating frequencies of hundreds of kHz).

Weakly coupled micro-mechanical resonators are highly prone to structural asymmetries induced by manufacturing tolerances. The presence of small imperfections in an array of identically designed resonators leads to a distortion in the vibration mode shape from the case of a structurally symmetric system [4]. The vibration energy becomes spatially localized and does not extend uniformly throughout the structure [5]. This effect often results in non-uniform reductions in R_x from the case of perfect symmetry [6]. While it is possible to tune the structural symmetry and consequently improve conformity in R_x reduction [3][6], this method still remains impractical for larger 1D-κ arrays.

Alternative design methodologies have been investigated to help improve the immunity of such coupled arrays to the impact of manufacturing tolerances in the context of their application to micro-electro-mechanical filters. More specifically, two-dimensional coupling [7] [8] [9] and [10], higher order [11] as well as cyclic coupling architectures [12] and [13] have been shown experimentally and numerically to provide improved insertion loss and ripple characteristics, indicating an enhancement in robustness against vibration localization effects relative to their 1D-κ counterparts. Similarly a cross coupled topology [14] has been shown to improve the robustness of the R_x to external stiffness perturbations compared to the traditional 1D-κ chain.

In an attempt to obtain a better scalability and more predictable R_x reduction of such weakly coupled arrays, this paper presents a numerical study of the impact of manufacturing tolerances on the achievable R_x for different classes of mechanical coupling topologies: one-dimensional coupling (1D-κ, Fig. 1a), two-dimensional coupling (2D-κ, Fig. 1b), cyclic-coupling (C-κ, Fig. 1c) and cross-coupling (X-κ, Fig.

A. Erbes, P. Thiruvenkatanathan, J. Woodhouse and A. A. Seshia are with the Department of Engineering, University of Cambridge, Cambridge, CB2 1PZ, U.K., and also with the Nanoscience Center, University of Cambridge, Cambridge, CB3 0FF, U.K. (e-mail: aas41@cam.ac.uk).

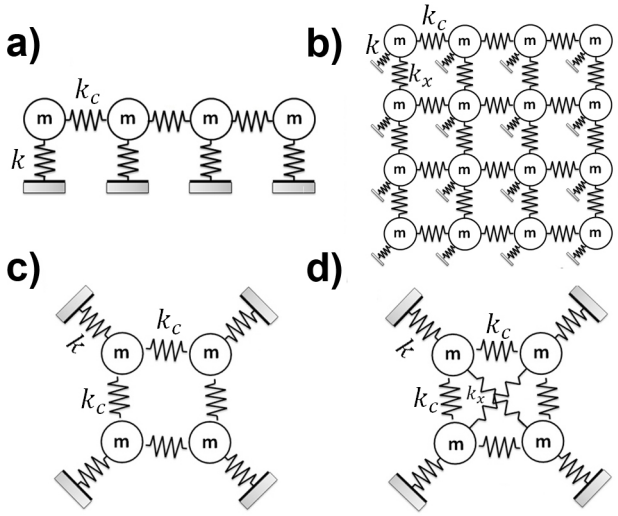

Fig. 1. Schematics of the equivalent mechanical models of the a) 1D-κ one dimensional coupled chain, b) 2D-κ coupling, c) C-κ cyclic-coupling and d) X-κ coupled configuration, respectively, for the special case of N = 4 resonators.

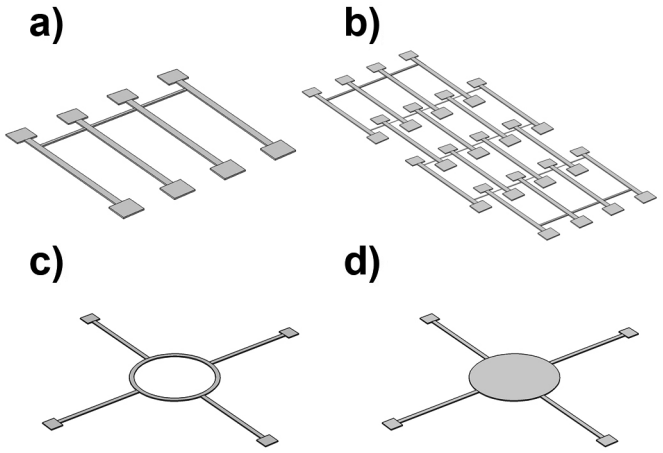

Fig. 2. Schematics of possible implementations of the a) 1D-κ one dimensional coupled chain, b) 2D-κ coupling, c) C-κ cyclic-coupling and d) X-κ coupled configuration, respectively, using flexural mode clamped-clamped beam resonators.

1d). The numerical study is based on a flexural mode Si MEMS double-ended-tuning fork (DETF) resonator operating at 250 kHz as described in [15] where the normalized inter-resonator spring coupling is experimentally quantified to be κ = k_c/k = 5x10^{-3}. In order to assess the robustness against process-induced variations, Monte Carlo numerical simulations, which accounted for up to $\pm$ 0.75 $\%$ random variations in resonator beam widths (with nominal value of 6 μm), were initiated to produce R_x estimates of the different coupling schemes. The coupling strength κ was varied over five orders of magnitude ($\kappa = 10^{-5}$ to $\kappa = 1$) for up to N = 40 coupled resonators. These results demonstrated that even small process variations can result in significant deviation from expectation.

II. Theory

A. System modeling

The degree of vibration energy confinement in a mechanically coupled array depends on the magnitude of the structural perturbations [4] as well as the strength of the internal coupling spring constant κ [16]. One possible approach to improving device immunity to structural perturbations is to increase the number of paths for the vibration energy to propagate within the system. To investigate this, we consider four classes of mechanical coupling topologies:

1) The traditional one dimensional chain (1D-κ) as shown in Fig. 1a with adjacent coupling k_c and free-ends at the edges
2) Two-dimensional square arrays (2D-κ) as shown in Fig. 1b with horizontal coupling k_c and vertical coupling k_x
3) Cyclic-coupling (C-κ) as shown in Fig. 1c, with adjacent coupling k_c throughout the array
4) Cross-coupling (X-κ) as shown in Fig. 1d with adjacent coupling k_c and non adjacent coupling k_x

These four distinct mechanical coupling schemes investigated in this paper differ from each other by their stiffness matrices K_{1D}, $K_{C-\kappa}$, K_{2D} and $K_{X-\kappa}$ for the 1D-κ, C-κ, 2D-κ and X-κ topologies, respectively.

Figure 2 shows schematics of possible implementations of the a) 1D-κ one dimensional coupled chain, b) 2D-κ coupling, c) C-κ cyclic-coupling and d) X-κ coupled configuration, respectively, using flexural mode clamped-clamped beam resonators. The topology of Fig. 2d has been practically implemented in [14] using a DETF configuration. Additional coupling paths can be implemented by using resonators coupled to a common base as it is the case in Fig. 2d. As the number of resonators is scaled up, the non-adjacent coupling terms vanish leading to a C-κ scheme described in Fig. 2c. The 2D-κ scheme on the other hand is scalable and is most suitable for alternative resonator designs (e.g. BAW squares, rings, etc.).

B. Modal analysis

We consider N mechanically coupled resonators (N^2 in the case of the 2D-κ architecture) each represented by a single-degree-of-freedom system with nominal mass m_0, stiffness k and damping coefficient c. In the case of electrostatically transduced MEMS resonators, we define the forcing vector $\mathbf{f}_m$ having zeros for all entries except the mth, which has harmonic forcing $f_m e^{j\omega t}$ where $f_m = \frac{C_0}{g} V_{DC} v_{ac}$ [15]. While we choose to treat the specific case of electrostatic transduction of the micro-resonators, the same analysis and modal approach presented in this section can be applied to any coupled resonator array regardless of the transduction scheme.

A discrete system with N degrees of freedom executing linear vibration behavior about a position of stable equilibrium and with damping governed by a dissipation matrix obeys the

governing equations

$$\mathbf{M}\ddot{\mathbf{y}}_\mathbf{m} + \mathbf{C}\dot{\mathbf{y}}_\mathbf{m} + \mathbf{K}\mathbf{y}_\mathbf{m} = \mathbf{f}_\mathbf{m} \tag{1}$$

The complex valued amplitude response vector $\mathbf{y_m}$ of the system can be computed as

$$\mathbf{y_m}(j\omega) = [-\omega^2\mathbf{M} + j\omega\mathbf{C} + \mathbf{K}]^{-1}\mathbf{f_m} \tag{2}$$

The transfer function of (2) has been used in [15] to obtain R_x distributions for different coupling topologies. In order to evaluate the total motional current at a resonance mode, a separate numerical frequency sweep is required to locate the exact peak amplitude distribution of $\mathbf{y_m}(j\omega)$. The N motional currents are then added together and the R_x is found. For large array sizes, this numerical method does not scale well and simulation time can become very lengthy. For such situations, modal analysis can be used to enable faster numerical simulation to provide more insight on the impact of array scaling. We demonstrate that the R_x expression is dependent on the eigenvector (i.e. mode shape) of the mode of vibration. In order to formulate the modal analysis, we follow the results obtained in [17] for the general case of coupled resonators.

The undamped natural frequencies ω_n and corresponding mode shape vectors $\mathbf{u}^{(n)}$ of (1) can be found by solving:

$$\mathbf{K}\mathbf{u}^{(n)} = \omega_n^2\mathbf{M}\mathbf{u}^{(n)},\ n = 1, ..., N \tag{3}$$

where the real-valued eigenvectors are mass-normalized as

$$\mathbf{u}^{(n)t}\mathbf{M}\mathbf{u}^{(n)} = 1,\ n = 1, ..., N \tag{4}$$

We then define the projected damping matrix as

$$\mathbf{C'} = [\mathbf{u}^{(1)}...\mathbf{u}^{(N)}]^t\mathbf{C}[\mathbf{u}^{(1)}...\mathbf{u}^{(N)}] \tag{5}$$

The displacement vector $\mathbf{y_m}$ for the damped case can be written as a linear combination of the eigenvectors

$$\mathbf{y_m} = \sum_{k=1}^{N} q_{k,m}\mathbf{u}^{(k)}e^{j\omega t} \tag{6}$$

Substituting (6) into (1) and simplifying gives

$$[\mathbf{A} + j\omega\mathbf{C''}]\mathbf{q}_m = \mathbf{Q}_m \tag{7}$$

where

$$\mathbf{A} = diag[\omega_k^2 + j\omega C_{kk}^{'} - \omega^2],\ k = 1, ..., N \tag{8}$$

$$\mathbf{q}_m = [q_{1,m}...q_{N,m}]^t \tag{9}$$

$$\mathbf{Q}_m = f_m[u_m^{(1)}u_m^{(2)}...]^t \tag{10}$$

and **C''** is **C'** with the diagonal elements deleted. From the standard expansion

$$(\mathbf{A} + j\omega\mathbf{C''})^{-1} \approx \mathbf{A}^{-1} - j\omega\mathbf{A}^{-1}\mathbf{C}''\mathbf{A}^{-1} \tag{11}$$

we can evaluate the $q_{k,m}$ coefficients as

$$q_{k,m} \approx \frac{f_m u_m^{(k)}}{(\omega_k^2 + j\omega C'_{kk} - \omega^2)} - j\omega\sum_{i\neq k}\frac{f_m C'_{ki}u_m^{(i)}}{(\omega_k^2 + j\omega C'_{kk} - \omega^2)(\omega_i^2 + j\omega C'_{ii} - \omega^2)} \tag{12}$$

To use the mechanically coupled resonators as a single entity, all of the N masses are actuated together. We therefore write the net forcing vector $\mathbf{F}$ as

$$\mathbf{F} = \sum_m \mathbf{f}_m,\ m = 1, ..., N \tag{13}$$

The total displacement response $\mathbf{Y}$ is then

$$\begin{aligned}\mathbf{Y} = [Y_1...Y_N]^t &= \sum_m \mathbf{y_m} \\ &= \sum_m\sum_k q_{k,m}\mathbf{u}^{(k)}e^{j\omega t} \\ &= e^{j\omega t}\sum_k \mathbf{u}^{(k)}\left(\sum_m q_{k,m}\right)\end{aligned} \tag{14}$$

C. Motional Resistance R_x

Now that we have obtained an expression of the displacements within the array using (14), we can evaluate the estimated R_x for two particular modes of vibration located at the band edges: the lowest and highest eigenfrequencies. In this analysis we assume that the sensing and driving electrodes are located at the maximum displacement amplitude loci of the resonator and identical for all N. For other resonator topologies and more complex modes of vibration, a surface integration of the mode-shape is required in order to formulate the true generated motional current [18], which will not change the impact of vibration localization on the motional resistance.

Furthermore, the subsequent analysis assumes that all the eigenmodes have equal modal Q and identical damping matrices.

1) Operating at the lowest eigenfrequency: Suppose that we operate the coupled resonators in the first eigenmode (i.e. $\omega = \omega_1$). The forcing vector is written as

$$\mathbf{F} = f[1...1]^t \tag{15}$$

In the case of electrostatically transduced MEMS resonators, we define the total current I_{out} generated by the N time-varying capacitances as

$$I_{out} = j\omega_1\frac{C_0}{g}V_{DC}\sum_m Y_m \tag{16}$$

Assuming low modal overlap due to the high Q of MEMS resonators, the displacement vector $\mathbf{y_m}$ of (6) simplifies to

$$\mathbf{y_m} \approx q_{1,m}\mathbf{u}^{(1)}e^{j\omega_1 t} \tag{17}$$

where

$$q_{1,m} \approx \frac{f u_m^{(1)}}{(\omega_1^2 + j\omega_1 C'_{11} - \omega_1^2)} = \frac{f u_m^{(1)}}{(j\omega_1 C'_{11})} \tag{18}$$

This leads to a total displacement vector

$$\mathbf{Y} = \mathbf{u}^{(1)}e^{j\omega_1 t}\sum_m q_{1,m} = \mathbf{u}^{(1)}e^{j\omega_1 t}\frac{f}{(j\omega_1 C'_{11})}\sum_m u_m^{(1)} \tag{19}$$

and the total motional current resulting

$$I_{out} = j\omega_1 \left(\frac{C_0}{g}V_{DC}\right)^2 \frac{1}{(j\omega_1 C'_{11})} \left(\sum_m u_m^{(1)}\right)^2 v_{ac}e^{j\omega_1 t} = \frac{1}{C'_{11}} \left(\frac{C_0}{g}V_{DC}\right)^2 \left(\sum_m u_m^{(1)}\right)^2 v_{ac}e^{j\omega_1 t} \tag{20}$$

The motional resistance R_x is then defined as

$$R_x = \frac{v_{ac}}{|I_{out}|} = \frac{C'_{11}}{\left(\frac{C_0}{g}V_{DC}\right)^2 \left(\sum_m u_m^{(1)}\right)^2} \tag{21}$$

As perturbations are introduced in the coupled system, the mode shape begins to exhibit spatial localization. From (21), we see that the R_x of the coupled system is closely dependent on the degree of vibration localization through $\left(\sum_m u_m^{(1)}\right)^2$. It can be shown using the Cauchy-Schwarz inequality that this sum is maximized when the normalized mode shape is found as $\bar{u}_m^{(1)} = \frac{1}{\sqrt{N}}$ for all m. For the first eigenmode, this maximum is achievable and occurs when the system is structurally symmetric. Any deviation from structural symmetry results in a degradation in R_x.

2) Operating at the highest eigenfrequency: We now operate the coupled structure at the highest eigenfrequency (i.e. when $\omega = \omega_N$). To trigger this mode, the force vector is defined as:

$$\mathbf{F} = f\left[1..(-1)^{i+1}..(-1)^{N+1}\right]^t \tag{22}$$

Assuming again high Q and low modal overlap, we can re-write (6) as

$$\mathbf{y_m} \approx q_{N,m}\mathbf{u}^{(N)}e^{j\omega_N t} \tag{23}$$

where

$$q_{N,m} \approx (-1)^{m+1} f \frac{u_m^{(N)}}{(j\omega_N C'_{NN})} \tag{24}$$

This results in a total displacement vector $\mathbf{Y}$

$$\mathbf{Y} = \mathbf{u}^{(N)}e^{j\omega_N t} \frac{f}{(j\omega_N C'_{NN})} \sum_m (-1)^{m+1} u_m^N \tag{25}$$

In order to add all the motional currents in phase, the individual biasing electrodes of the resonators are chosen such that

$$I_{out} = j\omega_N \frac{C_0}{g}V_{DC} \sum_i (-1)^{i+1} Y_i = \frac{1}{C'_{NN}} \left(\frac{C_0}{g}V_{DC}\right)^2 \left(\sum_i (-1)^{i+1} u_i^N\right)^2 v_{ac}e^{j\omega_N t} \tag{26}$$

Because of the nature of the highest eigenfrequency,

$$\sum_i (-1)^{i+1} u_i^N = \sum_i |u_i^N| \tag{27}$$

The sum of (27) is also maximized when all the individual components of the eigenvector $\mathbf{u}^{(N)}$ are equal.However, because of the coupling spring, this particular mode intrinsically exhibits a localization of the vibration distribution. The absolute amplitude of vibration is minimal on the edges of the chain and gradually increases to a maximum value at the centre of the structure [10]. Therefore the normalized eigenvector of the highest eigenfrequency cannot achieve:

$$\bar{\mathbf{u}}^{(N)} = \frac{1}{\sqrt{N}}\left[1..(-1)^{i+1}..(-1)^{N+1}\right]^t,\ N > 2 \tag{28}$$

The R_x of the coupled system when operated at ω_N is therefore not minimized when the system is structurally symmetric. In the case of composite-array resonators the lowest eigenfrequency appears to be the best choice in order to minimize the R_x of coupled MEMS resonators. All the following results will assume operation at $\omega = \omega_1$.

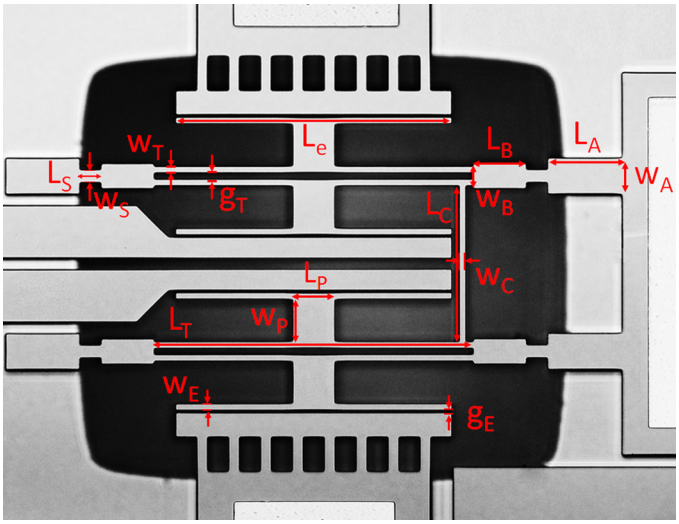

Fig. 3. Optical micrograph of two identically designed mechanically coupled DETF resonators used as a building block of the numerical simulations.

III. Numerical Simulations

In order to quantify the robustness of the distinct coupling schemes in the face of process-induced variations, numerical simulations were based on electrostatically transduced (transduction gap of 2μm) double-ended-tuning-fork resonators (DETF) presented in [6] operating at the fundamental in-phase tuning fork mode at 250 kHz and achieving a Q of 30000 in vacuum conditions. An optical micrograph of two mechanically coupled DETF resonators is shown in Fig. 3. The dimensional details of the particular mechanically coupled DETF design are summarized in Table I. The value of the mechanical coupling spring κ was experimentally quantified using the curve-veering phenomenon [16] by electrostatically tuning the mechanical stiffness of one of the resonators, while keeping all other structural parameters constant [15].

Monte Carlo numerical simulations, which accounted for up to 0.75 % random variations in resonator beam widths, were initiated to produce R_x estimates of the four coupling schemes for up to $N = 40$ resonators. These random variations were achieved numerically by setting the beam width b_i of the ith resonator as

TABLE I. DESIGN PARAMETERS

DETF tine width w_T	6 μm
DETF tine length L_T	300 μm
DETF separation g_T	6 μm
Base width w_B	24 μm
Base length L_B	50 μm
Stub width w_S	12 μm
Stub length L_S	20 μm
Anchor width w_A	34 μm
Anchor length L_A	70 μm
Coupling beam width w_C	5 μm
Coupling beam length L_C	145 μm
Plate width w_P	40 μm
Plate length L_P	40 μm
Electrode width w_E	6 μm
Electrode length L_E	260 μm
Electrostatic gap g_E	2 μm
Device thickness	25 μm

$$b_i = b_0\left(1 + \mathcal{N}(0,\sigma)\right) \tag{29}$$

where b_0 is the nominal value of the beam width, $\mathcal{N}(0,\sigma)$ is the normal distribution with zero mean and standard deviation 3σ = 7.5x10^{-3} (i.e. 99.7 $\%$ of the random beam widths generated are within 45 nm from their nominal value b_0 = 6 μm).

Choosing these values allows for 2.25 $\%$ of random variations in the resonator stiffness k which can considerably affect the vibration dynamics of such high-Q, weakly coupled resonator systems. Randomly modifying the beam widths of the DETF tines allows us to simulate breaks in structural symmetry due to both mass and stiffness perturbations. The DETF frequency follows a normal distribution with a mean of 247.6 kHz and standard deviation σ = 770 Hz (i.e. 3100 ppm variation). In order to return motional resistance values expected from experimental measurements while allowing for the resonators to operate in the linear region, a polarization voltage V_{DC} = 10V is specified.

IV. RESULTS

In order to understand the importance of the coupling strength and array size, we generate contour plots of the mean (μ) and standard deviation (σ) of the R_x (kΩ) distributions for different combinations of array sizes (N) and normalized coupling strengths (κ). For each $(N_i;\kappa_i)$ position in the plot, we evaluate the R_x distribution over $N_{random} \geq 1000$ cases and return the required performance measures. In this section we use the full expression of the $q_{k,m}$ linear coefficients found in (12) to obtain the R_x of the arrays.

A. Contour plots: 1D-κ scheme

Figures 4a and Fig. 4b show the contour plots of the mean and standard deviation of the R_x, respectively, in the case of the 1D-κ topology.

From Fig. 4a we see that for a given κ, increasing N improves μ, with the fastest reduction occurring when $\kappa \geq 10^{-2}$.

For the particular case κ = 5x10^{-3}, we see that when $N \geq 10$ the mean R_x levels off, indicating that at one point the chain becomes large enough so that only a small number of resonators (N_{active}), vibrate out of the total N. The remaining ones have vibration amplitudes close to null and therefore do not contribute to the generation of motional current and overall decrease in R_x. For this particular resonator topology and coupling strength, having more than 10 coupled resonators is not beneficial towards decreasing the R_x.

For a given chain length N, the mean can be improved by using larger κ values. This is to be expected since the variations in the eigenstates (δu_n) resulting from normalized stiffness perturbations $\left(\delta_k = \frac{\Delta k_i}{k}\right)$ are inversely proportional to κ [16] as shown in the case of two coupled resonators

$$\left|\frac{\delta u_n}{u_n}\right| \propto \frac{\delta_k}{4\kappa} \tag{30}$$

Such variations δu_n will modify the sum $\left(\sum_m u_m^{(1)}\right)^2$ and consequently affect the R_x of the array-composite resonator.

For $\kappa \leq 10^{-3}$, there is no clear advantage in coupling more resonators towards a decrease of the mean R_x.

In the case of the spread in R_x at κ = 5x10^{-3}, we see from Fig. 4b that the largest σ occurs for chains of 5-10 resonators. From that point on, the standard deviation slowly decreases as the number of resonators increases. This can be explained by the fact that for larger array sizes, since only N_{active} resonators are vibrating, the spread in the overall R_x will be dictated by the spread of the active resonators - those that are not vibrating will not contribute anymore to the overall spread. As N becomes very large, the number of participating resonators drops even further and the σ approaches that of a single resonator.

From Fig. 4b we see that the smallest σ values appear in clearly defined regions of the $(N_i;\kappa_i)$ space. The region of large σ occurs for values of κ close to 10^{-3} and therefore from (30), changes in eigenvectors become significant when $\delta_k \approx 4\kappa$. For this particular topology, Monte Carlo simulations allow for up to 2.25 $\%$ variations in k of a given resonator (from the nominal case) - the largest σ values can therefore be expected in the vicinity of $\kappa = 10^{-3} - 10^{-2}$.

B. Contour plots: C-κ scheme

Figures 4c and Fig. 4d show the contour plots of the mean and standard deviation of the R_x, respectively, in the case of the C-κ topology. Comparing Fig. 4a and Fig. 4c, we notice that the μ distributions are similar for both coupling schemes. The C-κ has a slightly shifted contour plot towards lower κ values indicating a decrease in vibration localization as compared to the 1D-κ for a given coupling strength.

From Fig. 4d we see an improvement in the standard deviation plots as the width of large σ zones are slightly smaller than those for the 1D-κ case. This suggest an improved immunity of this coupling scheme to external perturbations.

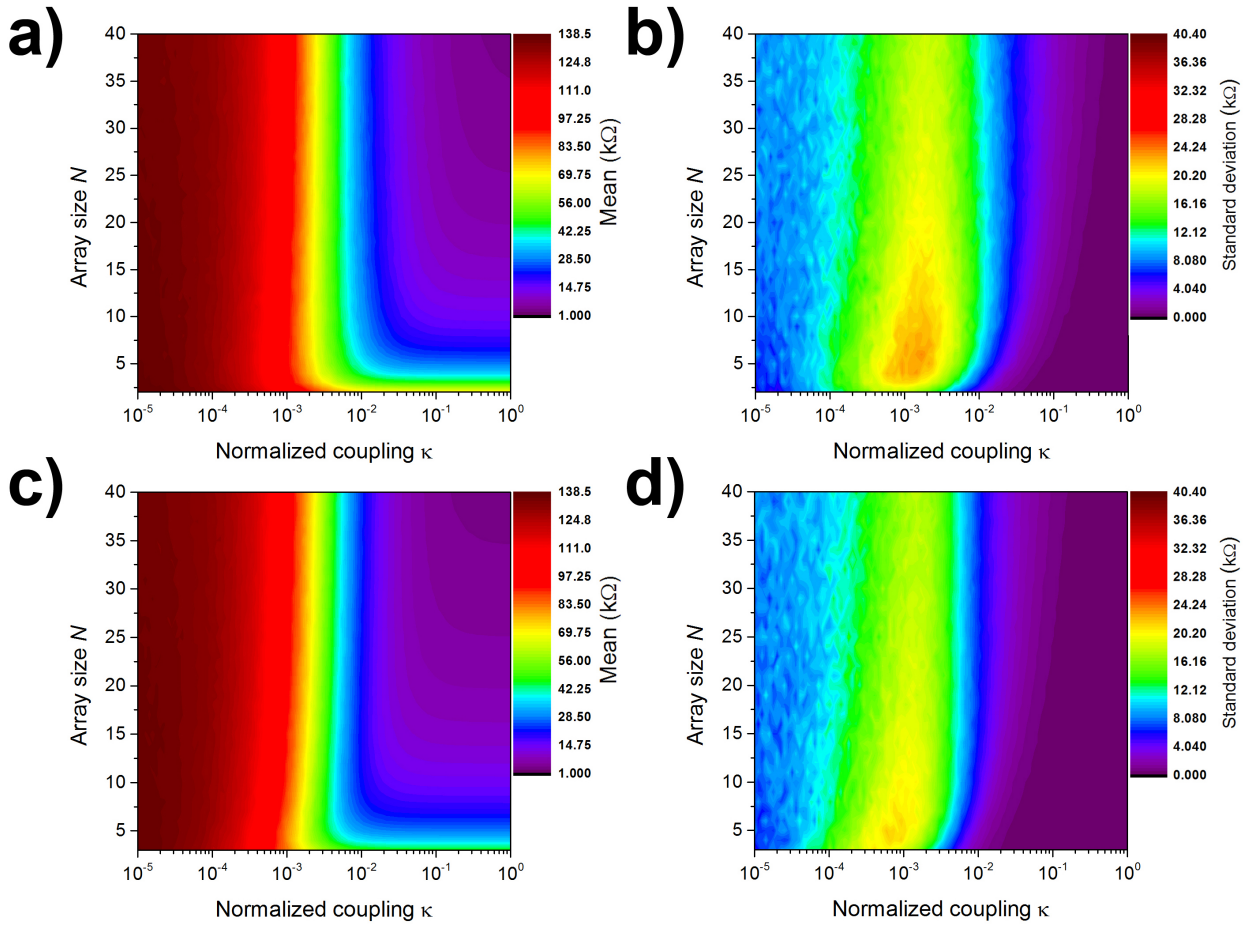

Fig. 4. Contour plots of the a) Mean (μ) and b) Standard deviation (σ) of the R_x (kΩ) for the 1D-κ case. Contour plots of the c) μ and d) σ for the C-κ case.

C. Contour plots: X-κ with $\kappa_x = \frac{\kappa}{10}$

Figures 5a and Fig. 5b show the contour plots of the mean and standard deviation of the R_x, respectively, of the X-κ topology for the particular case where the non-adjacent coupling is $\kappa_x = \frac{\kappa}{10}$. The X-$\kappa$ is a useful numerical coupling topology to investigate the importance of the additional non-adjacent coupling on the overall performance. It also exhibits a different behavior in the μ variations as N is increased, compared to 1D-κ and C-κ schemes. We see from Fig. 5a that the width of large μ zones shrinks as N gets large. This behavior is similar for the σ contours (Fig. 5b). Therefore, this coupling scheme offers improved immunity to process variations in terms of R_x scaling.

D. Contour plots: 2D-κ with $\kappa_x = \kappa$

While the X-κ scheme is useful for numerical studies, it remains challenging to implement this scheme for large N. A scheme in which additional adjacent and non-adjacent coupling can be implemented is the 2D array scheme. In this case we consider square arrays of dimension NxN and assume a horizontal coupling κ and vertical coupling $\kappa_x = \kappa$ (as found in Fig. 1b. Figures 5c and Fig. 5d plot the contours for the μ and σ respectively. Compared to the 1D-κ and C-κ cases, there is a clear shift of the contour plots towards lower κ values for both the μ and σ. However, the maximum spread is significantly larger compared to the other schemes. Furthermore from Fig. 5d, when $\kappa \geq 10^{-2}$, increasing N does not lead to a significant increase in σ as reported in the 1D-κ and C-κ schemes. There is a critical value of κ for which the system because quasi-immune to external perturbations in terms of the R_x variation. One can use these contour plots to estimate the critical coupling factors required to obtain process-tolerant coupled resonators.

Table II summarizes some extracted R_x means and standard deviations achieved by the different coupling schemes for N = 25 total number of resonators (i.e. 5x5 array in the 2D-κ case). From Table II it can be seen that the 2D-κ scheme is not the most optimal one in terms of reducing the variation in R_x as compared to the traditional 1D-κ in low κ regimes (i.e. $\kappa < 10^{-2}$). However, as soon as $\kappa \geq 10^{-2}$, the mean and spread is reduced by 75 $\%$ as compared to the 1D-κ scheme. In the very weak coupling regimes, the C-κ achieves a 20 $\%$ reduction in spread compared to the 1D-κ at identical mean values of R_x. Thus, the contour plots can effectively inform the optimization

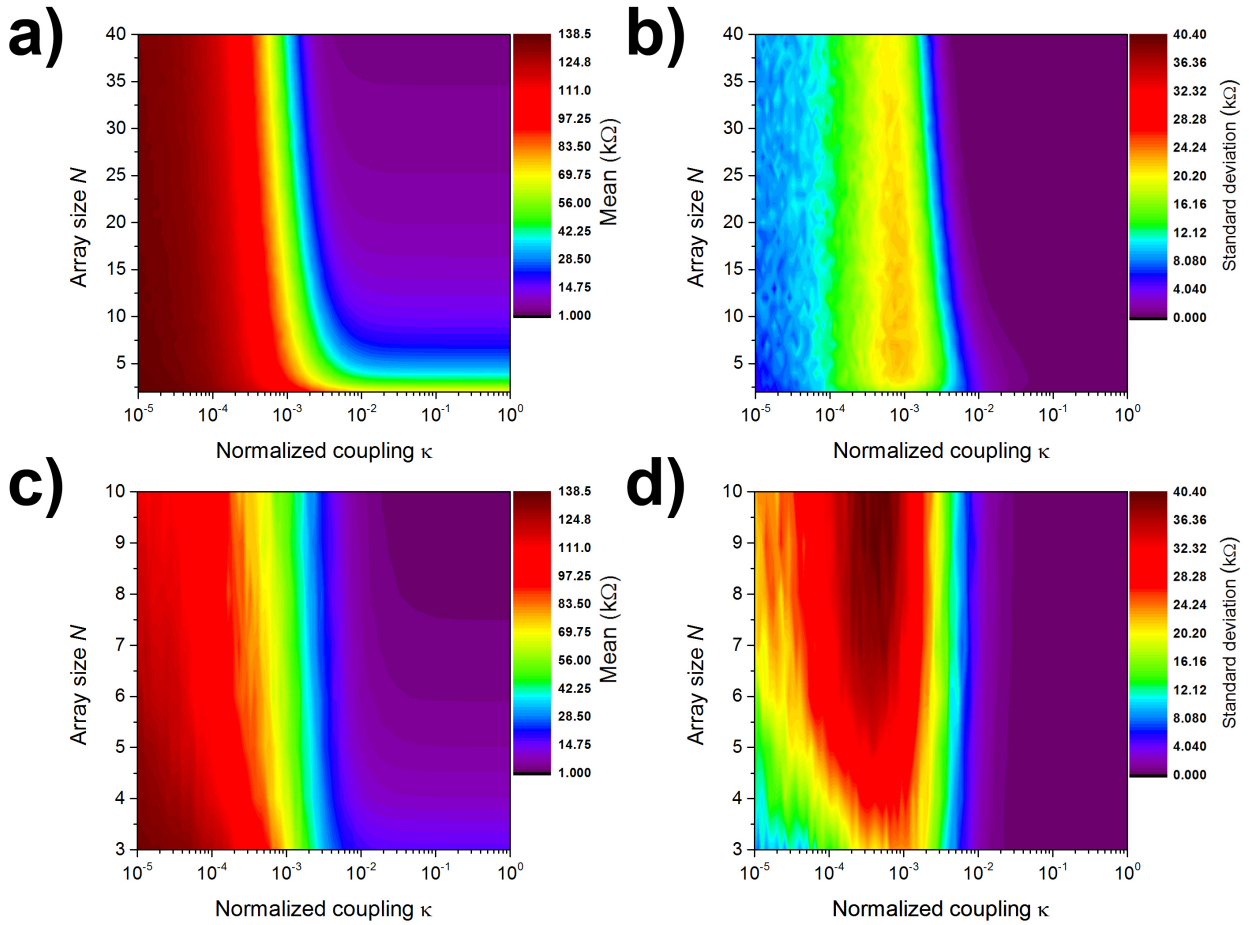

Fig. 5. Contour plots of the a) Mean (μ) and b) Standard deviation (σ) of the R_x (kΩ) for the X-κ case. Contour plots of the c) μ and d) σ for the 2D-κ case.

TABLE II. MEAN AND STANDARD DEVIATION OF THE R_x FOR N= 25 TOTAL NUMBER OF RESONATORS

κ		10^{-5}	10^{-4}	10^{-3}	10^{-2}	10^{-1}	1
1D-κ	μ (kΩ)	135.61	130.53	96.36	26.74	7.78	5.64
	σ (kΩ)	8.74	9.78	17.43	11.48	2.09	0.062
C-κ	μ (kΩ)	135.96	130.49	93.63	20.78	5.88	5.39
	σ (kΩ)	6.97	9.24	18.21	6.34	0.41	0.007
2D-κ	μ (kΩ)	128.84	103.00	57.52	6.590	3.91	3.89
	σ (kΩ)	14.34	31.83	29.77	2.89	0.029	0.003
X-κ	μ (kΩ)	135.11	123.34	44.65	5.79	5.62	5.62
	σ (kΩ)	8.00	11.54	19.81	0.086	0.005	0.004

procedure for coupled resonator architectures by identifying the critical coupling strength values and arrays sizes which directly improve the robustness of the R_x to manufacturing variations.

E. Frequency variations

From the previous sections we see that higher order coupling schemes improve the variation in R_x. Similarly we can investigate the robustness of the series resonance frequency of such array-composites. Figure 6 plots the standard deviation of the frequency variation σ_f defined as $\left(\frac{f_i - f_0}{f_0}\right)$ in ppm for the a) 1D-κ, b) C-κ, c) X-κ (with $k_x = k_c/10$) and d) 2D-κ (with $k_x = k_c$) topologies, as a function of the array size and coupling strength κ. From Figure 6 we see that the maximum frequency variation is 2200-3000 ppm and occurs for small array sizes. These values are consistent with the Monte Carlo simulation scheme used which allows up to roughly 0.3 % variation in natural frequency for a single resonator. From these plots we observe that as we go from the 1D-κ to the X-κ topology, the large σ_f domains are skewed to lower κ values, that is, for a given array size, the frequency variation improves as the coupling coefficient is increased. For a given coupling strength, using larger array sizes diminishes the variations in the frequencies. These results are consistent with what we would expect and what has been reported in the field [10], [19] and [9]. Furthermore once again, the 2D-κ is the most practical implementation to actively reduce the frequency variations to external perturbations.

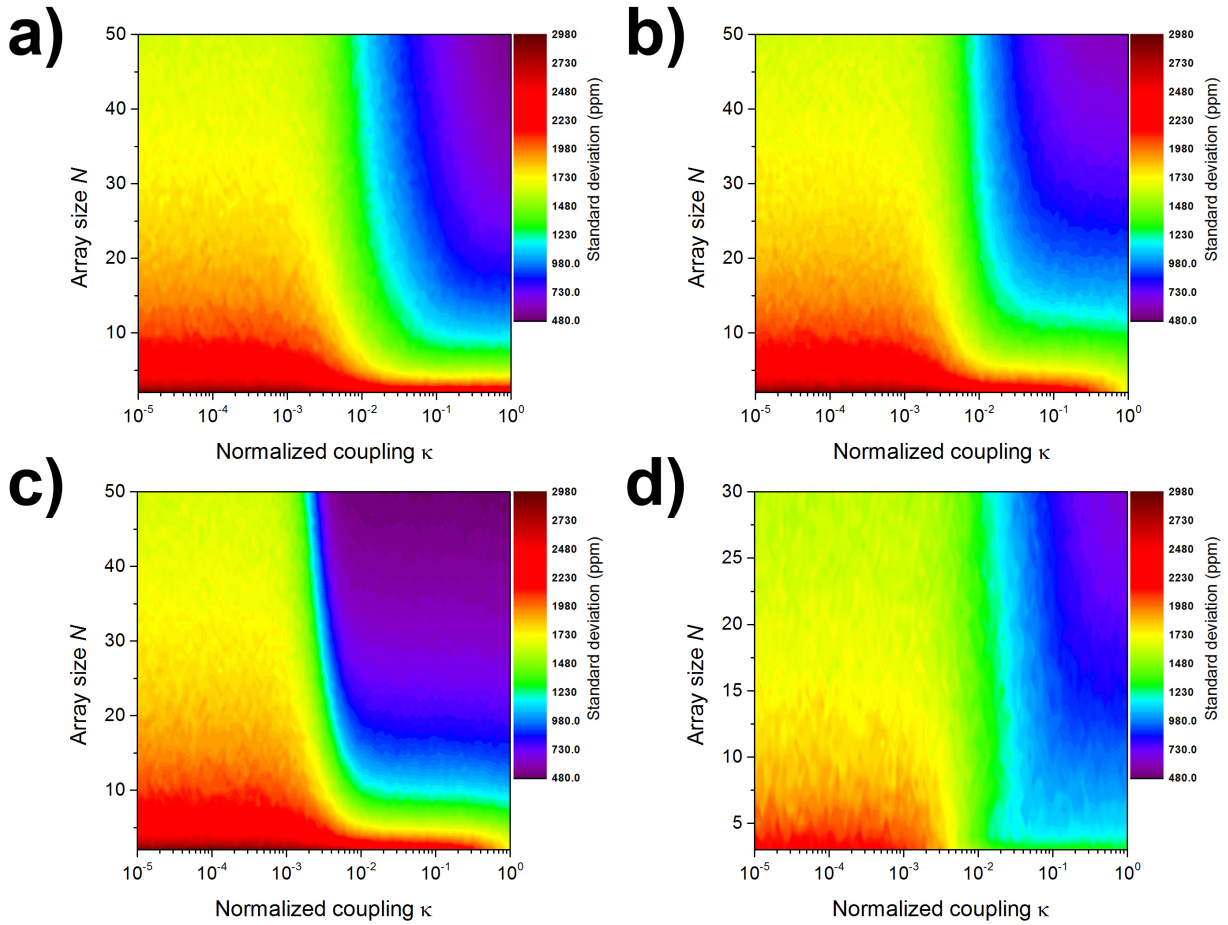

Fig. 6. Contour plots of the standard deviation σ_f of the frequency variation $\left(\frac{f_i - f_0}{f_0}\right)$ in ppm for the a) 1D-κ, b) C-κ, c) X-κ (with $k_x = k_c/10$) and d) 2D-κ (with $k_x = k_c$) case.

V. Conclusion

This paper presents the study of the impact of process and structural variations on the motional resistance of four distinct mechanical coupling topologies of MEMS resonators. The achievable R_x of mechanically coupled MEMS resonators is largely dependent on the chosen resonator topology, coupling scheme, coupling strength, array size and magnitude of structural perturbations. From the modal analysis of mechanically coupled resonators, we derive the dependence of the overall R_x measure to the vibratory mode-shape. In the presence of process variations, these mode-shapes deviate from the case of structurally symmetric solutions and induce vibration localization, which has a detrimental effect on the R_x. It is possible however to minimize these effects even in the case of weakly coupled structures by employing alternative coupling topologies.

The numerical trends, based on Monte Carlo simulation methods and relatively large Q such that modal-overlap remains low, suggest an improvement in the mean and spread of R_x as the number of coupled resonators N is increased for the X-κ scheme as opposed to the traditional 1D-κ linear chain and the cyclic C-κ configuration. The 2D-κ topology appears to be a good candidate as it is a relatively simple and practical coupling scheme which is able to achieve more predictable R_x reductions than the standard 1D chain.

The numerical method developed in this paper provides a quick and simple design procedure to evaluate the structural immunity to process variations for a given set of performance metrics (in this case the overall R_x) of coupled MEMS resonators. Since the simulations rely on a traditional modal analysis, more complex resonator topologies and mode shapes can be investigated in terms of R_x and frequency distributions in face of process variations. These numerical results motivate in-depth studies of alternative coupling topologies, in the case of weakly coupled resonators, towards designing process tolerant, highly scalable array-composite resonators.

For a given resonator topology and coupling scheme, these simulation plots based on modal-analysis can be used to predict the behavior of large arrays and provide design guidelines to select the appropriate κ and N values to achieve the required R_x even when process variations are significant.

ACKNOWLEDGMENT

The authors would like to gratefully acknowledge the Qualcomm European Research Studentships in Technology and the UK Engineering and Physical Sciences Research Council.

REFERENCES

[1] C. T.-C. Nguyen, "MEMS technology for timing and frequency control," *Ultrasonics, Ferroelectrics and Frequency Control, IEEE Transactions on*, vol. 54, no. 2, pp. 251 –270, february 2007.

[2] M.U. Demirci and C. T.-C. Nguyen, "Mechanically corner-coupled square microresonator array for reduced series motional resistance," *Microelectromechanical Systems, Journal of*, vol. 15, no. 6, pp. 1419 –1436, dec. 2006.

[3] M. Akgul, Z. Ren, and C. T.-C. Nguyen, "Voltage-controlled tuning to optimize MEMS resonator array-composite output power," in *Frequency Control and the European Frequency and Time Forum (FCS), 2011 Joint Conference of the IEEE International*, may 2011, pp. 1 –6.

[4] C. Pierre, "Mode localization and eigenvalue loci veering phenomena in disordered structures," *Journal of Sound and Vibration*, vol. 126, no. 3, pp. 485 – 502, 1988.

[5] P. Thiruvenkatanathan, J. Woodhouse, J. Yan, and A. Seshia, "Manipulating vibration energy confinement in electrically coupled micro-electromechanical resonator arrays," *Microelectromechanical Systems, Journal of*, vol. 20, no. 1, pp. 157–164, Feb 2011.

[6] A. Erbes, P. Thiruvenkatanathan, and A. Seshia, "Impact of mode localization on the motional resistance of coupled MEMS resonators," in *Frequency Control Symposium (FCS), 2012 IEEE International*, 2012, pp. 1–6.

[7] D. Weinstein, S. Bhave, M. Tada, S. Mitarai, and S. Morita, "Mechanical coupling of 2D resonator arrays for MEMS filter applications," in *Frequency Control Symposium, 2007 Joint with the 21st European Frequency and Time Forum. IEEE International*, 2007, pp. 1362–1365.

[8] J. A. Judge, B. H. Houston, D. M. Photiadis, and P. C. Herdic, "Effects of disorder in one- and two-dimensional micromechanical resonator arrays for filtering," *Journal of Sound and Vibration*, vol. 290, no. 35, pp. 1119 – 1140, 2006.

[9] Y. Lin, W.-C. Li, B. Kim, Y.-W. Lin, Z. Ren, and C. T.-C. Nguyen, "Enhancement of micromechanical resonator manufacturing precision via mechanically-coupled arraying," in *Frequency Control Symposium, 2009 Joint with the 22nd European Frequency and Time forum. IEEE International*, April 2009, pp. 58–63.

[10] C. Kharrat, E. Colinet, L. Duraffourg, S. Hentz, P. Andreucci, and A. Voda, "Modal control of mechanically coupled NEMS arrays for tunable rf filters," *Ultrasonics, Ferroelectrics and Frequency Control, IEEE Transactions on*, vol. 57, no. 6, pp. 1285–1295, June 2010.

[11] S.-S. Li, M. Demirci, Y.-W. Lin, Z. Ren, and C. T.-C. Nguyen, "Bridged micromechanical filters," in *Frequency Control Symposium and Exposition, 2004. Proceedings of the 2004 IEEE International*, Aug 2004, pp. 280–286.

[12] V. B. Chivukula and J. F. Rhoads, "Microelectromechanical bandpass filters based on cyclic coupling architectures," *Journal of Sound and Vibration*, vol. 329, no. 20, pp. 4313–4332, 2010.

[13] D. Greywall and P. Busch, "Coupled micromechanical drumhead resonators with practical application as electromechanical bandpass filters," *Journal of Micromechanics and Microengineering*, vol. 12, no. 6, pp. 925–938, 2002.

[14] A. Erbes, P. Thiruvenkatanathan, J. Yan, and A. Seshia, "Investigating vibration dynamics of cross-coupled MEMS resonators for reduced motional resistance," in *Solid-State Sensors, Actuators and Microsystems (TRANSDUCERS EUROSENSORS XXVII), 2013 Transducers Eurosensors XXVII: The 17th International Conference on*, June 2013, pp. 1711–1714.

[15] A. Erbes, P. Thiruvenkatanathan, and A. Seshia, "Numerical study of the impact of process variations on the motional resistance of weakly coupled MEMS resonators," in *European Frequency and Time Forum International Frequency Control Symposium (EFTF/IFC), 2013 Joint*, July 2013, pp. 674–677.

[16] P. Thiruvenkatanathan, J. Yan, J. Woodhouse, and A. Seshia, "Enhancing parametric sensitivity in electrically coupled MEMS resonators," *Microelectromechanical Systems, Journal of*, vol. 18, no. 5, pp. 1077 –1086, oct. 2009.

[17] J. Woodhouse, "Linear damping models for structural vibration," *Journal of Sound and Vibration*, vol. 215, no. 3, pp. 547 – 569, 1998.

[18] D. L. DeVoe, "Piezoelectric thin film micromechanical beam resonators," *Sensors and Actuators A: Physical*, vol. 88, no. 3, pp. 263 – 272, 2001.

[19] L. Wu, M. Akgul, W.-C. Li, Y. Lin, Z. Ren, T. Rocheleau, and C. T.-C. Nguyen, "Micromechanical disk array for enhanced frequency stability against bias voltage fluctuations," in *European Frequency and Time Forum International Frequency Control Symposium (EFTF/IFC), 2013 Joint*, July 2013, pp. 547–550.

Andreja Erbes received his MEng in 2011 and MA in 2014 in Electrical and Electronic Engineering from the Department of Engineering at the University of Cambridge. In 2009, he spent a year abroad at the Massachusetts Institute of Technology within the Cambridge-MIT Exchange Program and took part in an undergraduate-research opportunity program (UROP) under the supervision of Prof. D. Weinstein, working in the field of Micro-Electro-Mechanical-Systems (MEMS). He is currently pursuing his Ph.D. degree at the University of Cambridge under the supervision of Dr. Ashwin A. Seshia. His research includes the design of MEMS resonators and CMOS circuits for low power wireless communications and timing applications.

Pradyumna Thiruvenkatanathan received his B.E. in Electrical and electronics engineering from Anna University, Chennai, India in 2006, the M.Phil in Micro- and Nanotechnology Enterprise in 2007 and a Ph.D. in Micro-systems Engineering in 2011 both from the University of Cambridge, UK. Following his time as a graduate student, he spent two years as a post-doctoral research associate at the Cambridge Nanoscience centre and researched on methods of enhancing performance of micromechanical inertial sensors. He was affiliated to the Department of Engineering and Churchill College during his time at Cambridge.

Jim Woodhouse studied mathematics at the University of Cambridge (B.A. 1972), and stayed on there for PhD (1977) and postdoctoral studies, both related to the acoustics of the violin. After a spell working for a consultancy company, in 1985 he took up a post in the Engineering Department in Cambridge, and has been successively a lecturer, reader and professor there. His research interests cover a range of topics in structural vibration: friction-excited vibration such as vehicle brake squeal, acoustics of musical instruments, modelling of structural damping mechanisms, and vibration prediction methods for complex structures.

Ashwin A. Seshia received his BTech in Engineering Physics in 1996 from IIT Bombay, MS and PhD degrees in Electrical Engineering and Computer Science from the University of California, Berkeley in 1999 and 2002 respectively, and the MA from the University of Cambridge in 2008. During his time at the University of California, Berkeley, he was affiliated with the Berkeley Sensor & Actuator Center. He joined the faculty of the Engineering Department at the University of Cambridge in October 2002 where he is presently a Reader in Microsystems Technology and a Fellow of Queens' College. Ashwin's research interests are in the domain of micro-engineered dynamical systems with applications to sensors and sensor systems. He serves as Editor for the IEEE Journal of Microelectromechanical Systems and as Associate Editor for the IEEE Transactions on Ultrasonics, Ferroelectrics and Frequency Control.